Arabian Journal of Chemistry (2022) **15**, 104132

King Saud University

Arabian Journal of Chemistry

www.ksu.edu.sa
www.sciencedirect.com

ORIGINAL ARTICLE

A novel polysaccharide from *Paeonia lactiflora* exerts anti-tumor activity via immunoregulation

Xuelian Wang [a], Na Li [a,b], Ying Li [a], Yinan Zhao [a], Liang Zhang [c,*], Yanjun Sun [d], Yasushi Ohizumi [e], Jing Xu [a,*], Yuanqiang Guo [a,c,*]

[a] *State Key Laboratory of Medicinal Chemical Biology, College of Pharmacy, and Tianjin Key Laboratory of Molecular Drug Research, Nankai University, Tianjin 300350, People's Republic of China*
[b] *School of Chinese Materia Medica, Shenyang Pharmaceutical University, Shenyang 110016, People's Republic of China*
[c] *State Key Laboratory of Tea Plant Biology and Utilization, Anhui Agricultural University, Hefei 230036, People's Republic of China*
[d] *School of Pharmacy, Henan University of Chinese Medicine, Zhengzhou 450046, People's Republic of China*
[e] *Kansei Fukushi Research Institute, Tohoku Fukushi University, Sendai 989-3201, Japan*

Received 9 April 2022; accepted 13 July 2022
Available online 19 July 2022

KEYWORDS

Polysaccharide;
Anti-tumor activity;
Immunomodulatory activity;
RAW264.7;
Zebrafish;
Paeonia lactiflora

Abstract An unreported polysaccharide, PLP90-1B, was isolated from *Paeonia lactiflora*. Structural analysis showed that PLP90-1B contained arabinose and glucose, which was a highly-linear gluco-arabinan having a molecular weight of about 9.5 kDa. The backbone of PLP90-1B consisted of → 5)-α-L-Ara*f*-(1→, →3,5)-α-L-Ara*f*-(1→, →2,3,5)-α-L-Ara*f*-(1→, and → 4)-α-D-Glc*p*-(1→, terminating with α-L-Ara*f*. PLP90-1B was found to have anti-tumor activity by suppressing the proliferation and migration of HepG2 cells microinjected into the zebrafish. The further mechanism investigation revealed that the anti-tumor activity of PLP90-1B was closely related to immune regulation, which can improve phagocytic ability and enhance the release of NO and cytokines (IL-6, IL-1*β*, and TNF-α) in RAW264.7 cells. The immunopotentiation activity was further corroborated by zebrafish experiments. All these results exhibited that PLP90-1B may have the potential to become a potentially immune-mediated anti-tumor drug in the future.

1. Introduction

Polysaccharides are a kind of macromolecular polymers widely existing in nature, which have many pharmacological effects, such as anti-tumor (Cheng et al., 2020), immunoregulation (Bhardwaj et al., 2021), and anti-oxidation (Liu et al., 2021). These macromolecules have drawn an increasing number of attention in scientific researches and industrial applications owing to their unique physicochemical properties and

* Corresponding authors.
E-mail addresses: zhangliang@ahau.edu.cn (L. Zhang), xujing611@nankai.edu.cn (J. Xu), victgyq@nankai.edu.cn (Y. Guo).
Peer review under responsibility of King Saud University.

Production and hosting by Elsevier

https://doi.org/10.1016/j.arabjc.2022.104132
1878-5352

biological functions. Recently, a large number of studies on plant polysaccharides from *Caesalpinia bonduc*, *Cuminum cyminum*, and Ginseng etc. have shown that these macromolecules possess remarkable immuno-stimulatory properties (Mandal et al., 2013; Tabarsa et al., 2020). In addition, some homogeneous polysaccharides have been found to have anti-tumor activity. Zhang et al. (2021a) extracted a polysaccharide from *Rosa laevigata*, which had anti-tumor activity.

Tumors are caused by the abnormal proliferation of local tissues and cells stimulated by various tumorigenic factors and have extremely high morbidity and mortality. For the treatment of tumor, besides surgical treatment, chemotherapy is one of the commonly used methods. Unfortunately, chemotherapy drugs usually have certain side effects including cytotoxicity and damage to the immune system. Therefore, it is urgent to discover effective and low- or non-toxic agents for cancer treatment. Immunoregulation has been considered to be an important defense strategy for human body to prevent and fight against various diseases. Immunotherapy, which exerts efficacy by promoting immunity, has been employed clinically for cancer treatment (Sheng et al., 2022). Previous studies have demonstrated that lentinan could indirectly exert anti-tumor effects by enhancing immune responses of the host. In addition, the polysaccharides from *Tarphochlamys affinis* (Tang et al., 2016) and *Strongylocentrotus nudus* eggs (Xie et al, 2017) have also been found to perform anti-tumor effects through activating immune system. Therefore, it may be a potential strategy to discover immunostimulatory polysaccharides as anti-tumor agents.

The roots of *Paeonia lactiflora* Pall., have been used extensively in China, Korea, and Japan. In traditional Chinese medicines, the roots of *P. lactiflora* are frequently applied for calming liver, relieving pain, nourishing blood, regulating menstruation, and preventing perspiration. Clinically, the roots have been used to treat immune-related diseases (Han et al., 2021), influenza (Yu et al., 2021), and inflammation (Meng et al., 2021). The chemical composition analysis revealed that total glucosides of paeonia (TGP) were the main effective constituents of *P. lactiflora* (Han et al., 2021). Apart from small molecules, *P. lactiflora* polysaccharides and their biological effects including anti-oxidation, anti-tumor, anti-diabetes have also been widely concerned. Among these polysaccharides, most studies focused on the crude polysaccharides, and a few reports focused on the homogeneous polysaccharides in *P. lactiflora* (Zhang et al., 2020b). However, the research on the homogeneous polysaccharides in *P. lactiflora* is very limited, and the structures and biological activities of the homogeneous polysaccharides are worthy of further investigation.

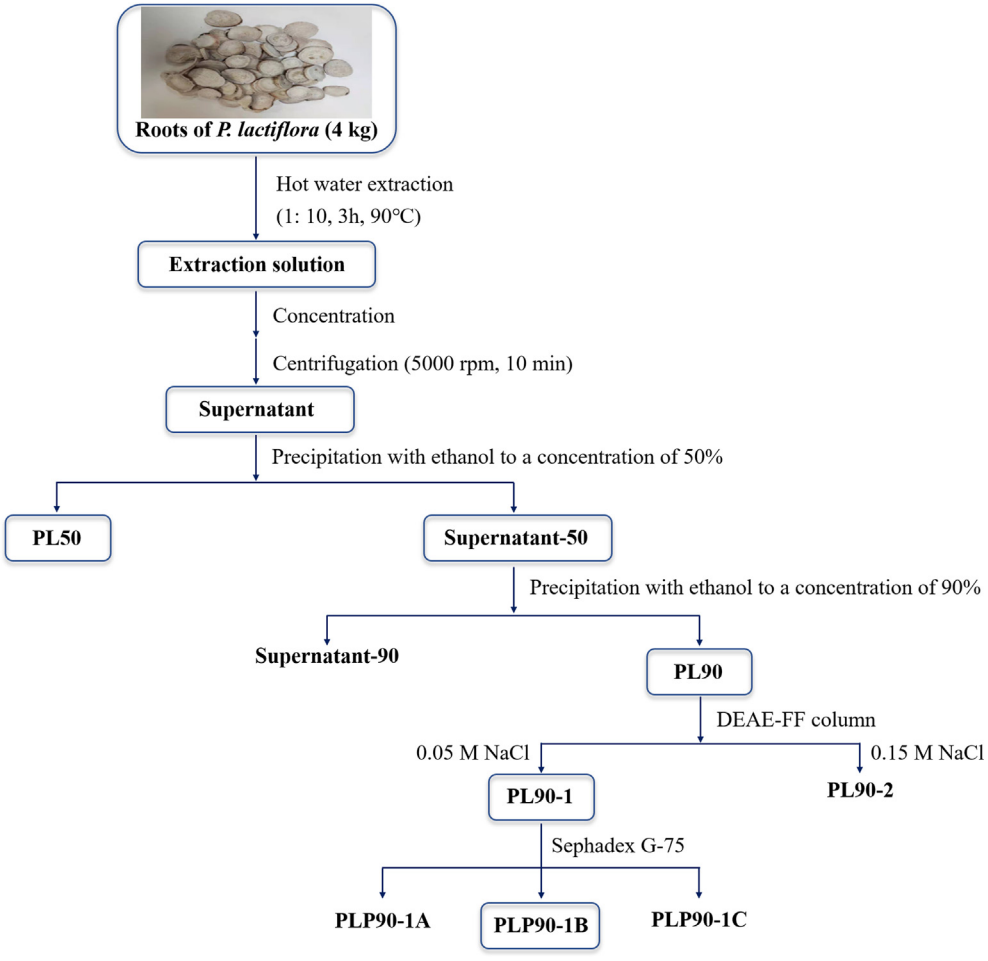

Fig. 1 The flow chart for the extraction and purification of polysaccharides from *P. lactiflora*.

Considering the extensive applications of the roots of *P. lactiflora* in clinical and the lack of its polysaccharide study, the current work is to investigate the homogeneous polysaccharides, including monosaccharide composition, structure elucidation, and physicochemical properties. Combining with the immunotherapy of cancer, the anti-tumor and immunomodulatory effects of the polysaccharide PLP90-1B were exploited using cells and zebrafish models.

2. Materials and methods

2.1. Materials and reagents

The materials and reagents are described in Supplementary methods S1.

2.2. Isolation and purification of PLP90-1B

Using hot water extraction, ethanol precipitation, and fractionation by DEAE-Sepharose Fast Flow (DEAE-FF) column and Sephadex G-75 column, a homogeneous polysaccharide PLP90-1B was obtained. The preparation process was shown in Fig. 1. The detailed procedures are presented in the Supplementary methods S2.

2.3. Structural characterization of PLP90-1B

2.3.1. Molecular weight and homogeneity determination

An Agilent 1260 HPLC system (Agilent, Washington, USA) equipped with TSK GEL G-5000PWXL and G-3000PWXL gel columns in series (Tosoh Biosep, Tokyo, Japan) and a Shodex RI-101 refractive index detector (Showa Denko, Tokyo, Japan) was used for detecting molecular weight of PLP90-1B (Hui and Gao, 2022). The detailed experimental processes are provided in the Supplementary methods S3.

2.3.2. Monosaccharide composition detection

The 1-phenyl-3-methyl-5-pyrazolone (PMP) precolumn derivatization method was employed for the analysis of monosaccharide composition of PLP90-1B (Zhang et al., 2020a). The explicit procedures are described in the Supplementary methods S4.

2.3.3. Absolute configuration analysis of monosaccharides

After determining the monosaccharide composition, absolute configuration of monosaccharides in PLP90-1B was determined by HPLC via comparison with standard samples. The specific processes are summarized in the Supplementary methods S5.

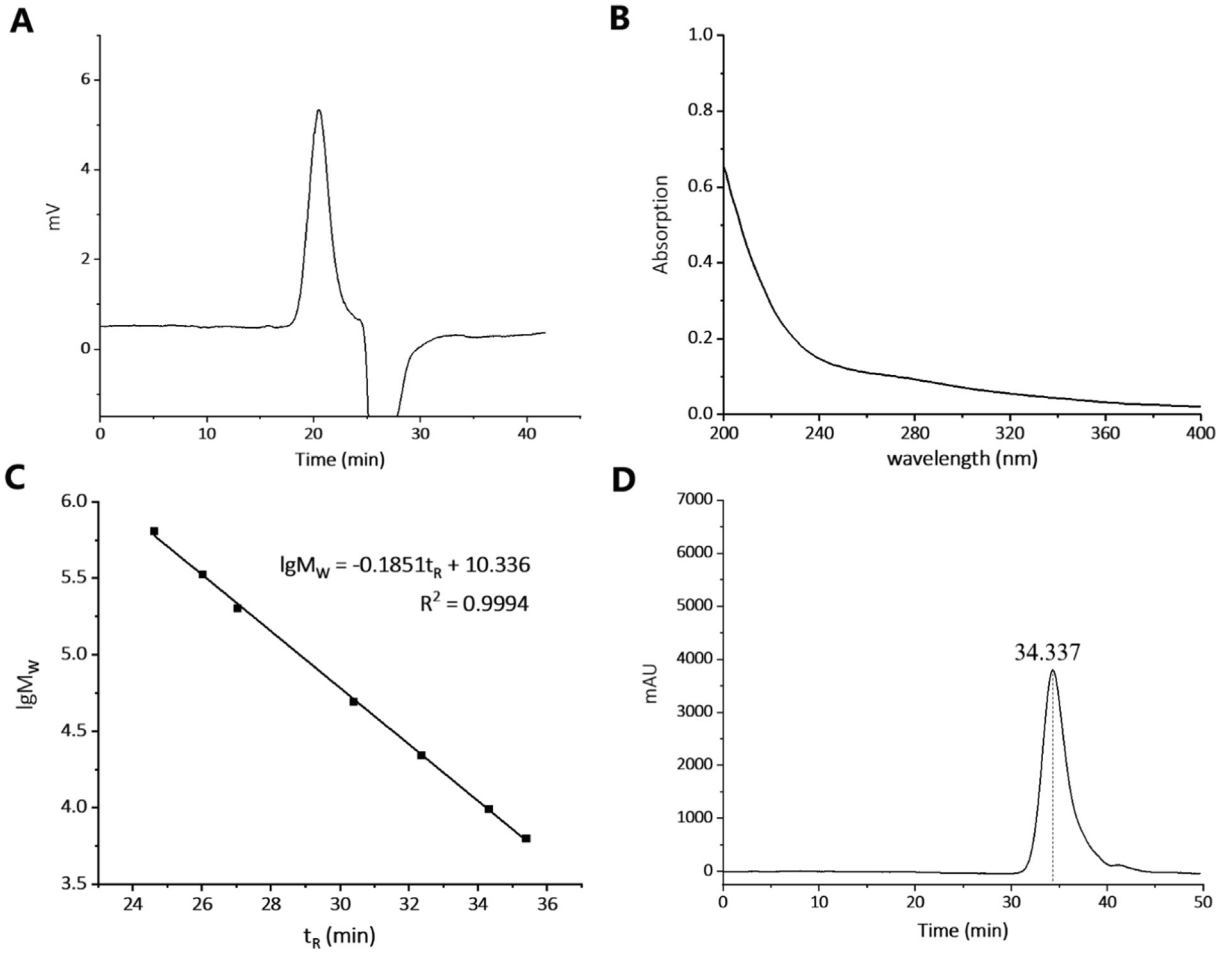

Fig. 2 Homogeneity and molecular weight analysis of PLP90-1B. (A) The HPGPC profile of PLP90-1B. (B) The UV spectrum of PLP90-1B. (C) The calibration curve of molecular weight of standards. (D) The HPSEC profile of PLP90-1B.

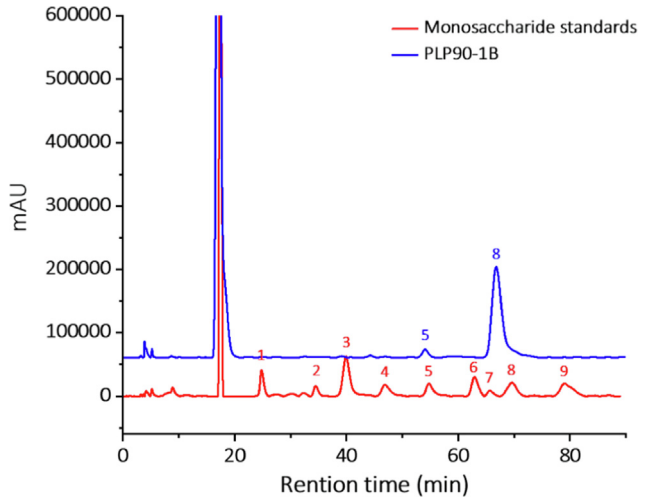

Fig. 3 The monosaccharide composition of PLP90-1B (1: mannose; 2: rhamnose; 3: glucuronic acid; 4: galacturonic acid; 5: glucose; 6: galactose; 7: xylose; 8: arabinose; 9: fucose).

2.3.4. Ultraviolet and Fourier-transform infrared spectra

The UV absorption peaks of a polysaccharide at 260 or 280 nm are usually used to determine whether the polysaccharide contains nucleic acid or protein (Molaei and Jahanbin, 2018). The PLP90-1B aqueous solution (1 mg/mL) was scanned from 200 nm to 400 nm with a UV–vis spectrophotometer (Youke, Shanghai, China). Deionized water was used as the blank.

PLP90-1B (2 mg) was blended with dry KBr powder (200 mg) and squashed as sheet (1 mm), which was subjected to a FT-IR spectrometer (Bruker, Ettlingen, Germany).

2.3.5. Methylation and GC–MS analysis

Methylation analysis was carried out as reported in the literature (Ciucanu and Kerek, 1984). Detailed process is supplemented in the Supplementary methods S6.

2.3.6. Nuclear magnetic resonance analysis

PLP90-1B (60 mg) was entirely dissolved in D_2O (550 μL, 99.9 %). The ^1H, ^{13}C, DEPT-135, HSQC, and HMBC were obtained on a 400 MHz Bruker spectrometer (Bruker, Ettlingen, Germany). Additionally, for ^1H NMR spectrum, the acquisition time (AQ) was set as 4.0895 s, the relaxation delay (d1) was set as 1.0000 s, the spectral width (SWH) was set as 8012.8 Hz, and the number of scans (NS) was set as 16. For ^{13}C NMR, the AQ, d1, SWH, and NS were set to 0.4999 s, 1.0000 s, 35714.3 Hz, and 8000, respectively. The parameters of HSQC and HMBC were set as default values.

2.3.7. Congo red assay

1 mg/mL of polysaccharide solution was blended with equal volume of Congo red solution, followed by adding NaOH solution (1 M) to adjust the final concentration of NaOH as 0, 0.1, 0.2, 0.3, 0.4, 0.5, and 0.6 M, respectively. Finally, the UV maximum absorption wavelength of each concentration between 400 and 600 nm was recorded.

2.4. In vivo anti-tumor effects of PLP90-1B

2.4.1. Zebrafish husbandry and maintenance

AB strain zebrafish (*Danio rerio*) were obtained from Shanghai Feixi Biotechnology Co., Ltd. (Shanghai, China). Adult AB zebrafish were maintained at 28.5 °C and reared in a 14 h light/10 h dark cycle. Sodium chloride (NaCl) and sodium bicarbonate ($NaHCO_3$) were taken to maintain the conductivity at 525 μs/cm and pH of fresh water was 7.2. Zebrafish embryos were derived from adult male and female zebrafish by mating at a ratio of 2: 1. Embryos were cultured in medium in an incubator (28.5 °C).

2.4.2. Anti-tumor activity evaluation using zebrafish xenograft model

The influences of PLP90-1B on the tumor cell proliferation and metastasis *in vivo* were assessed using a zebrafish xenograft model (Fan, et al., 2018). Details for zebrafish xenograft model establishment can be found in the Supplementary methods S7.

2.5. Anti-proliferation effects of PLP90-1B

2.5.1. Cell culture

HepG2 cells were acquired from Shanghai Institute of Biochemistry and Cell Biology, Chinese Academy of Sciences (Shanghai, China). HepG2 cells were cultured in Dulbecco's modified Eagle's medium (DMEM) containing 10 % fetal bovine serum (FBS), 1 % streptomycin/penicillin at 37 °C in a 5 % CO_2 atmosphere.

Table 1 GC–MS analysis of PLP90-1B.

PMAAs	Major mass fragments (*m*/*z*)	Linkages	Molar ratio
1,4-di-*O*-acetyl-1-deuterio-2,3,5-tri-*O*-methyl-L-arabinitol	59, 71, 87, 102, 118, 129, 145,161	→1)-L-Ara*f*	7.13
1,4,5-tri-*O*-acetyl-1-deuterio-2,3-di-*O*-methyl-L-arabinitol	59, 71, 87, 102, 118, 129, 145, 162, 173, 189	→5)-L-Ara*f*-(1→	5.74
1,3,4,5-tetra-*O*-acetyl-1-deuterio-2-*O*-methyl-L-arabinitol	59, 74, 85, 99, 118, 127, 141, 159, 173, 187, 201, 217, 261	→3,5)-L-Ara*f*-(1→	6.67
1,2,3,4,5-penta-*O*-acetyl-1-deuterio-L-arabinitol	57, 73, 86, 103, 115, 128, 145, 159, 176, 188, 201, 218, 290	→2,3,5)-L-Ara*f*-(1→	1.28
1,4,5-tri-*O*-acetyl-1-deuterio-2,3,6-tri-*O*-methyl-D-glucitol	57, 71, 87, 102, 118, 129, 142, 162, 173, 203, 233	→4)-D-Glc*p*-(1→	1.00

2.5.2. In vitro anti-proliferation assay

The anti-proliferation activity of PLP90-1B was explored by MTT assay (Zhang et al., 2022b). Details are shown in the Supplementary methods S8.

2.6. Immunomodulatory effects of PLP90-1B in vitro

2.6.1. Cell culture

RAW264.7 cells were obtained from Shanghai Institute of Biochemistry and Cell Biology, Chinese Academy of Sciences (Shanghai, China). RAW264.7 cells were cultivated with standard conditions.

2.6.2. Cell viability determination using MTT assay

The cell viability of PLP90-1B on RAW264.7 cells was assessed using MTT assay (Zhang et al., 2022b). The exhaustive experimental procedures are summarized in the Supplementary methods S9.

2.6.3. Determination of phagocytic activity by neutral red assay

The effects of PLP90-1B on the phagocytic ability of RAW264.7 cells were assessed using a neutral red uptake assay (Shi et al., 2020). The overall processes are summarized in the Supplementary methods S10.

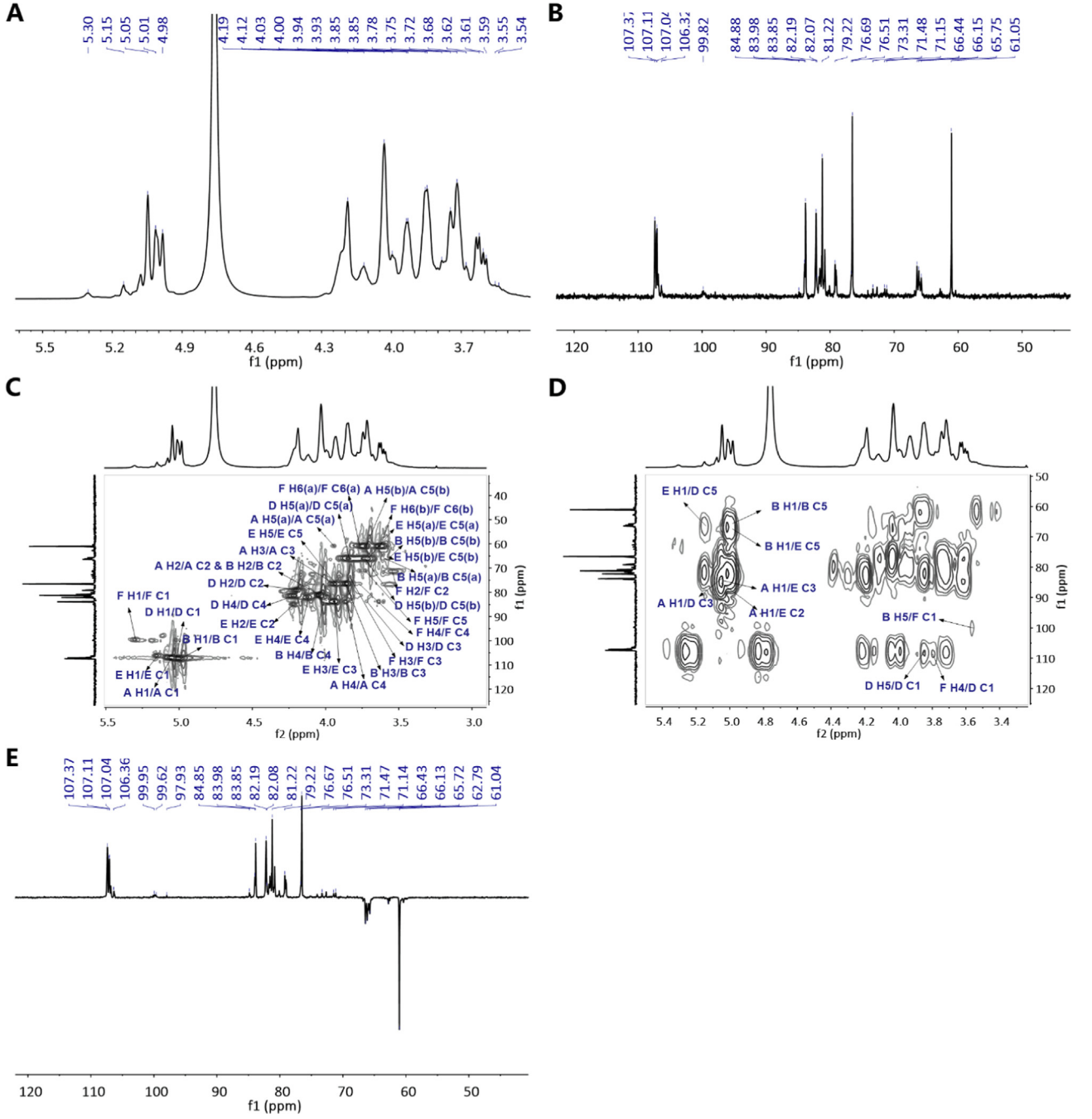

Fig. 4 NMR spectra of PLP90-1B. (A) ^{1}H NMR spectrum. (B) ^{13}C NMR spectrum. (C) HSQC spectrum. (D) HMBC spectrum. (E) DEPT-135 spectrum.

2.6.4. Measurement of nitric oxide (NO) in RAW 264.7 cells

The release of NO in RAW264.7 cells was measured by Griess assay (Zhu et al., 2022). The NO level was calculated by the standard curve of sodium nitrite ($NaNO_2$). Detailed experimental procedures are described in the Supplementary methods S11.

2.6.5. Determination of cytokines in RAW264.7 cells

The levels of cytokines including TNF-α, IL-6, and IL-1β in RAW264.7 cells were measured by the enzyme-linked immunosorbent assay (ELISA) kits according to the manufacturer's instructions. The detailed experimental steps are shown in the Supplementary methods S12.

2.7. Immunomodulatory effects of PLP90-1B in vivo

The immunoregulatory activity of PLP90-1B *in vivo* was evaluated using the levels of reactive oxygen species (ROS) and NO in the zebrafish model, in which DCFH-DA (3-amino, 4-aminomethyl-2′,7′-difluorescein diacetate) and DAF-FMDA (2,7-dichlorofluorescein diacetate) fluorescent probe dyes were used (Ko et al., 2019). The detailed processes are provided in the Supplementary methods S13.

2.8. Statistical analysis

Data were analyzed by Origin 8.0 software (OriginLab, USA) and expressed as the mean ± SD. Probabilities (P) < 0.05 were determined to be significant by analysis of variance (ANOVA). The differences among three or more groups were analyzed by one-way ANOVA Turkey's multiple comparison tests.

3. Results and discussion

3.1. Extraction, purification, and homogeneity analysis of PLP90-1B

A fraction of water-soluble crude polysaccharide PL90 was acquired from the roots of *P. lactiflora* with a yield of 0.83 %. PL90 was further isolated by DEAE-FF column and Sephadex G-75 column to afford a fraction PLP90-1B. The elution process of PL90 and PL90-1 were displayed in Fig. S1. In Fig. 2A, PLP90-1B was found to be a single and symmetrical peak in the chromatogram, which illustrated that it was a homogeneous polysaccharide. According to the retention time (t_R) and the calibration curve of standards, the molecular weight was calculated to be approximately 9.5 kDa (Fig. 2C–D). In addition, there were no peaks at 260 nm or 280 nm in the UV spectrum, suggesting that PLP90-1B did not have proteins or nucleic acids.

3.2. Monosaccharide composition and absolute configuration analysis of PLP90-1B

The monosaccharide composition of PLP90-1B was detected by HPLC. The results revealed that PLP90-1B consisted of arabinose (Ara) and glucose (Glc) in the molar ratio of 19.0: 1.0 by comparing with monosaccharide standards (Fig. 3). Moreover, Fig. S2 indicated that the absolute configurations of monosaccharides were L- and D-configurations.

3.3. FT-IR spectrum and methylation analysis of PLP90-1B

FT-IR spectrum can provide useful functional group information in polymers, which have been widely applied to characterize polysaccharides. As displayed in Fig. S3A, the strong absorption band at 3434 cm^{-1} was assigned to the stretching vibration of hydroxy groups (O−H). The absorption bands at 2930 cm^{-1} and 1459 cm^{-1} were ascribed to C−H stretching and C−H bending vibrations, respectively. The signal at 1636 cm^{-1} belonged to the vibration of water bond. The absorption peaks at 1109 and 1050 cm^{-1} were approximately ascribed to the asymmetric vibration of C−O−C or C−O−H bond (Wang et al., 2022). Additionally, the characteristic peak at 576 cm^{-1} revealed the presence of pyran ring.

Methylation analysis is one of the most powerful means to analyze the the position of glycosidic bonds. As showed in Fig. S3B, the vanishing of the characteristic peak at 3434 cm^{-1} confirmed the methylation of PLP90-1B exhaustive. Then, the methylated sample was hydrolyzed with acid, reduced by $NaBD_4$, and derivatized to give alditol acetates. The result displayed that PLP90-1B contained five different kinds of sugar residues, which were α-L-Ara*f*-(1→, →5)-α-L-Ara*f*-(1→, →3,5)-α-L-Ara*f*-(1→, →2,3,5)-α-L-Ara*f*-(1→, and → 4)-α-D-Glc*p*-(1→ (Fig. S4−S5). The relative molar ratio

Table 2 ^1H and ^{13}C NMR chemical shift assignments (δ in ppm) of PLP90-1B.

Sugar residues	C-1	C-2	C-3	C-4	C-5	C-6
	H-1	H-2	H-3	H-4	H-5	H-6
t-α-L-Ara*f*	107.0	81.2	76.5	83.9	61.1	-/-
Residue A	5.05	4.03	3.94	3.85	3.93/3.72	-/-
→5)-α-L-Ara*f*-(1→	107.4	81.2	76.5	82.2	65.8	-/-
Residue B	4.98	4.03	3.85	4.00	3.61/3.55	-/-
→3,5)-α-L-Ara*f*-(1→	107.1	79.2	83.9	81.2	66.2	-/-
Residue D	5.01	4.19	3.72	4.22	3.84/3.75	-/-
→2,3,5)-α-L-Ara*f*-(1→	106.3	84.9	84.0	82.1	66.4	-/-
Residue E	5.15	4.22	3.93	4.12	3.72/3.59	-/-
→4)-α-D-Glc*p*-(1→	99.8	71.5	73.3	76.7	71.2	61.1
Residue F	5.30	3.54	3.84	3.78	3.72	3.75/3.62

of PMAAs was 7.13: 5.74: 6.67: 1.28: 1.00. The linkages patterns of PLP90-1B were deduced and shown in Table 1.

3.4. NMR analysis of PLP90-1B

The structure of PLP90-1B were further analyzed by 1D and 2D NMR spectra. As shown in Fig. 4A−B, five anomeric signals at 4.98–5.30 and 99.8–107.4 ppm appeared in the ^{1}H and ^{13}C NMR spectra, which were consistent with the sugar residues in the GC–MS analysis. Additionally, to facilitate the determination of residues, five fragments were annotated as residues A, B, D, E, and F, respectively.

As shown in Fig. 4B, five anomeric carbon signals were observed clearly. According to the literature (Chen et al., 2019; Cheng et al., 2020; Li et al., 2020, 2021; Ma et al., 2019; Song et al., 2020; Wang et al., 2021a), the anomeric carbon signals at 107.4, 107.1, 107.0, and 106.3 ppm could be attributed to C−1 of 1,5-linked α-L-Ara*f* (residue B), 1,3,5-linked α-L-Ara*f* (residue D), t-linked α-L-Ara*f* (residue A), and 1,2,3,5-linked α-L-Ara*f* (residue E), respectively. The remaining anomeric

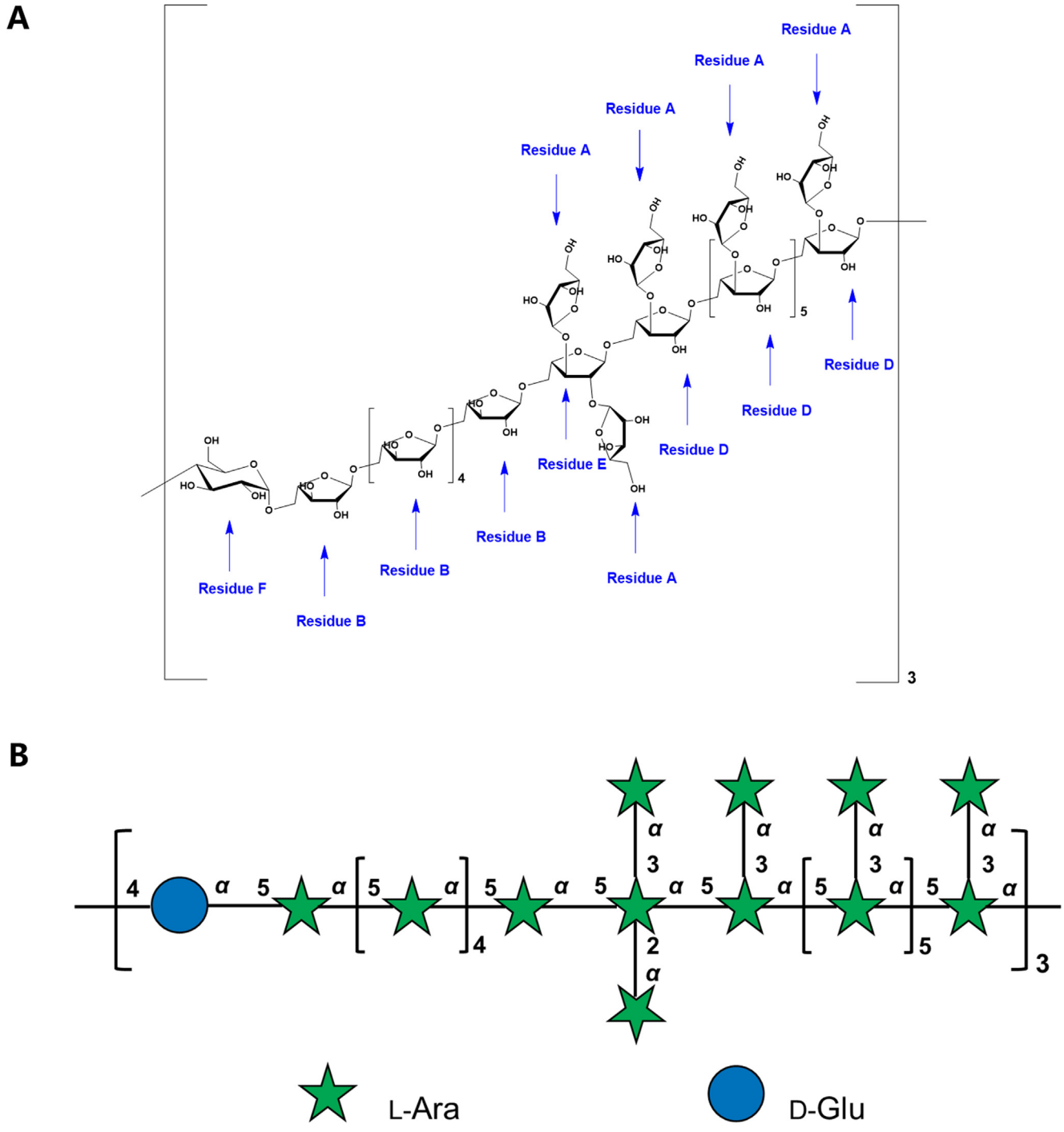

Fig. 5 The putative structure of PLP90-1B. (A) The structure of PLP90-1B represented with structural formula. (B) The structure of PLP90-1B represented with symbols.

signal at 99.8 ppm was ascribed to 1,4-linked α-D-Glc*p* (residue F). Moreover, according to the literature (Mandal et al., 2013; Patra et al., 2021; Shakhmatov et al., 2014; Wang et al., 2021b; Zhang et al., 2021b) and the analysis of DEPT-135 NMR spectrum (Fig. 4E), the inverted signals at 66.4, 66.2, 65.8, and 61.0 ppm could be attributed to C−5 of 1,2,3,5-linked α-L-Ara*f*, 1,3,5-linked α-L-Ara*f*, 1,5-linked α-L-Ara*f*, and t-linked α-L-Ara*f*, respectively. Concurrently, the inverted signal at 61.0 ppm belonged to C−6 of 1,4-linked α-D-Glc*p*. Further combining with the HSQC spectrum (Fig. 4C), 4.98, 5.01, 5.05, 5,15, and 5.30 ppm in the ^{1}H NMR spectrum (Fig. 4A) were relevant with C−1 of 1,5-linked α-L-Ara*f* (107.4 ppm), 1,3,5-linked α-L-Ara*f* (107.1 ppm), *t*-linked α-L-Ara*f* (107.0 ppm), 1,2,3,5-linked α-L-Ara*f* (106.3 ppm) and 1,4-linked α-D-Glc*p* (99.8 ppm), respectively. After assigning the anomeric signals of five sugar residues, the remaining proton signals in each residue of PLP90-1B were further determined by analyzing the ^{1}H, ^{13}C, HSQC, and HMBC spectra. All these signals were summarized in Table 2.

Furthermore, the HMBC spectrum was applied to confirm the monosaccharide sequence and linkage sites among the fragments. As shown in Fig. 4D, a cross-peak at 3.55/99.8 ppm (B H−5/F C−1) revealed that *O*-5 of residue B was attached at C-1 of residue F. Similarly, the correlation signals at 4.98/66.4 ppm (B H−1/E C−5), 5.15/66.2 ppm (E H−1/D C−5), and 3.78/107.1 ppm (F H−4/D C−1) revealed that *O*−1 of residue B was linked to C−5 of residue E, *O*−1 of residue E was linked to C−5 of residue D, and *O*−4 of residue F was linked to C-1 of residue D, respectively. The correlation signals at 5.05/83.9 ppm (A H−1/D C−3), 5.05/84.0 ppm (A H−1/E C−3), 5.05/84.9 ppm (A H−1/E C−2) exhibited that *O*−1 of residue A was linked to C−3 of residue D, *O*−1 of residue A was attached at C−3 of residue E, *O*−1 of residue A was attached at C−2 of residue E, respectively. In addition, the correlation signals at 4.98/65.8 ppm (B H−1/B C−5) and 3.84/107.1 ppm (D H−5/D C−1) indicated that residue B and residue D were present as repeated units in PLP90-1B (Wang et al., 2021b). Eventually, the NMR data authenticated that, as supported by the conclusions originated from methylation and monosaccharide composition analysis, the putative structure of PLP90-1B was deduced and displayed in Fig. 5.

3.5. Congo red assay of PLP90-1B

Congo red is an acid dye, which can engender a stable complex with polysaccharide with triple-helix structure. In general,

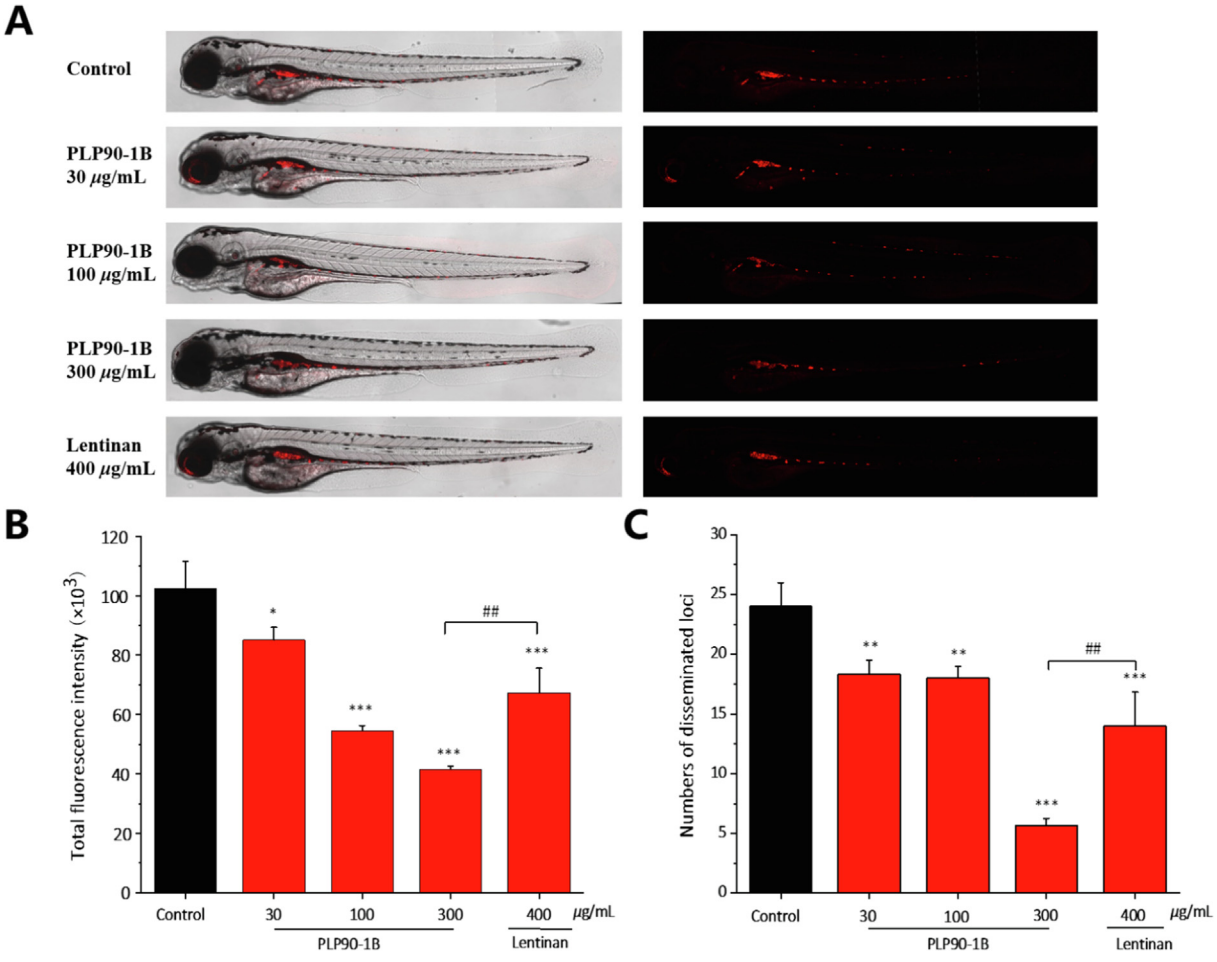

Fig. 6 *In vivo* anti-tumor effects of PLP90-1B in the zebrafish xenografts. (A) Intensity and distribution of the red fluorescence were imaged under a confocal microscope. (B) Fluorescence intensity of the tumor xenografts, representing HepG2 cell proliferation. (C) Quantification of the fluorescent area of the tumor xenografts, representing HepG2 cell metastasis. Results were expressed as means ± SD. $^{*}P < 0.05$, $^{**}P < 0.01$, $^{***}P < 0.001$ versus the control group; $^{\#\#}P < 0.01$ versus the lentinan group.

when the concentration of NaOH solution increases, the triple-helix conformation of polysaccharides will be destroyed under strong alkaline conditions, and the maximum absorption wavelength will decrease obviously in the UV–vis spectrum. As displayed in Fig. S6, no significant change in the maximum absorption wavelength of PLP90-1B-Congo red complex was observed when compared with pure Congo red, indicating that PLP90-1B had no triple-helix structure.

3.6. In vivo anti-tumor effects of PLP90-1B

3.6.1. Anti-tumor activity of PLP90-1B using zebrafish model

To find potentially bioactive macromolecules against cancer, PLP90-1B was assayed using a zebrafish tumor xenograft. As shown in Fig. 6, the cell proliferation (Fig. 6B) and migration (Fig. 6C) were significantly decreased after PLP90-1B treatment ($P < 0.05$). Furthermore, compared with the positive control, PLP90-1B at 300 μg/mL was more effective ($P < 0.01$). These findings indicated that PLP90-1B could suppress tumor cell multiplication and metastasis to exert anti-tumor effects.

3.6.2. The anti-proliferation activity of PLP90-1B

To examine whether the anti-tumor activity is related to cytotoxicity, the anti-proliferative activity of PLP90-1B was assayed using MTT assay. The cell viability after treatment with various concentrations of PLP90-1B was presented in Fig. S7. With the concentration increase, the inhibitory effects rose slightly, and the inhibition rates in different concentrations of PLP90-1B treated groups increased from 7.7 % (25 μg/mL) to 28.7 % (400 μg/mL). The above data indicated that PLP90-1B had no obvious anti-proliferative or cytotoxic activities, suggesting that the *in vivo* anti-tumor activity of PLP90-1B may not be closely related to the anti-proliferative effects.

3.7. Immunomodulatory effects of PLP90-1B

3.7.1. Effects of PLP90-1B on the viability and phagocytosis of RAW264.7 cells

The above zebrafish and cell experiments showed that the *in vivo* anti-tumor effects of PLP90-1B was not closely related to cytotoxicity. According to the newly emerged immunotherapy of cancer, which exerts efficacy by improving immunity, a series of immunomodulatory experiments were designed to reveal the possible anti-tumor mechanism.

As shown in Fig. 7A, there was no significant difference between PLP90-1B-treated and the blank control, which indicated that PLP90-1B (≤200 μg/mL) did not affect the cell survival. Therefore, the concentrations of PLP90-1B at 50, 100, and 200 μg/mL were used in the following immunomodulatory experiments.

Phagocytosis is an important feature of macrophage activation and an essential barrier for host to enhance innate immune system (Wang et al., 2020). As indicated in Fig. 7B, the phagocytic capacity treated with PLP90-1B or lipopolysaccharide (LPS, 1 μg/mL) was obviously stronger than the control group ($P < 0.01$), which increased by 17 %, 20 %, and 19 %, respectively.

3.7.2. Effects of PLP90-1B on the secretion of NO and cytokines in macrophages

NO is a cellular messenger with biological activity and participates in regulating apoptosis and defending against pathogens and tumor cells (Wang et al., 2018). Meanwhile, when macrophages are activated, the release of NO is raised, reflecting the

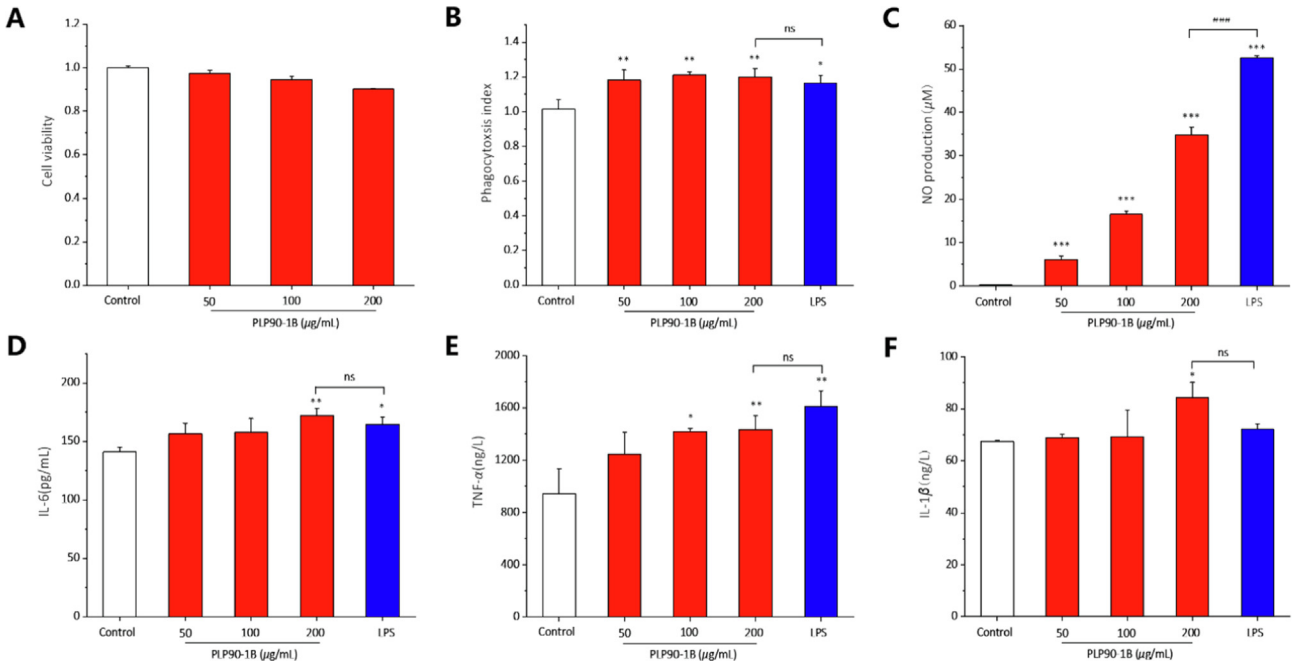

Fig. 7 Effects of PLP90-1B and positive control (LPS) on RAW264.7 cells. (A) Cell viability of RAW264.7 cells. (B) Phagocytic capacity of RAW264.7 cells. (C) NO production in RAW264.7 cells. (D) IL-6 levels in RAW264.7 cells. (E) TNF-α levels in RAW264.7 cells. (F) IL-1β levels in RAW264.7 cells. All values were presented as the mean ± SD of at least three independent experiments. *$P < 0.05$, **$P < 0.01$, ***$P < 0.001$ versus the control group; $^{\#\#\#}P < 0.001$ versus the LPS group; ns, no significance.

influence of polysaccharides on the immune response to exogenous substances. The influences of PLP90-1B on the level of NO production of RAW264.7 were presented in Fig. 7C. RAW264.7 macrophages treated with PLP90-1B released more NO production in concentration-dependent manner than the control group ($P < 0.001$).

In addition to NO, immune cells release multiple cytokines including IL-6, TNF-α, and IL-1β when intervened, which can prevent tumor cell invasion and microbial infection. Especially, TNF-α exexts multiple functions in acute or chronic inflammation, cell proliferation, and cell apoptosis (Zeinali et al., 2017). In this study, compared with the control group, all of the cytokines secreted by RAW264.7 cells rose slightly when the concentration of PLP90-1B rose from 50 to 200 μg/mL (Fig. 7D-F). Especially the release of TNF-α was dose-dependent ($P < 0.05$). The release of NO and cytokines of RAW264.7 cells stimulated by PLP90-1B demonstrated that PLP90-1B efficiently activated macrophages to exert the immunoregulatory function.

3.7.3. Effects of PLP90-1B on the production of NO and ROS in zebrafish embryos

Zebrafish has become an ideal animal model for *in vivo* experiments due to its numerous advantages, such as high transparency, rapid development, easy processing, and high homology with human genes. Additionally, as an important regulatory factor involved in various physiological processes, ROS not only increases the release of inflammatory cytokines, but also participates in innate immunity (Mohsenzadeh et al., 2021).

To further verify the immunostimulatory activity of PLP90-1B *in vivo*, the levels of ROS and NO in zebrafish embryos treated with PLP90-1B were detected. Corresponding to the

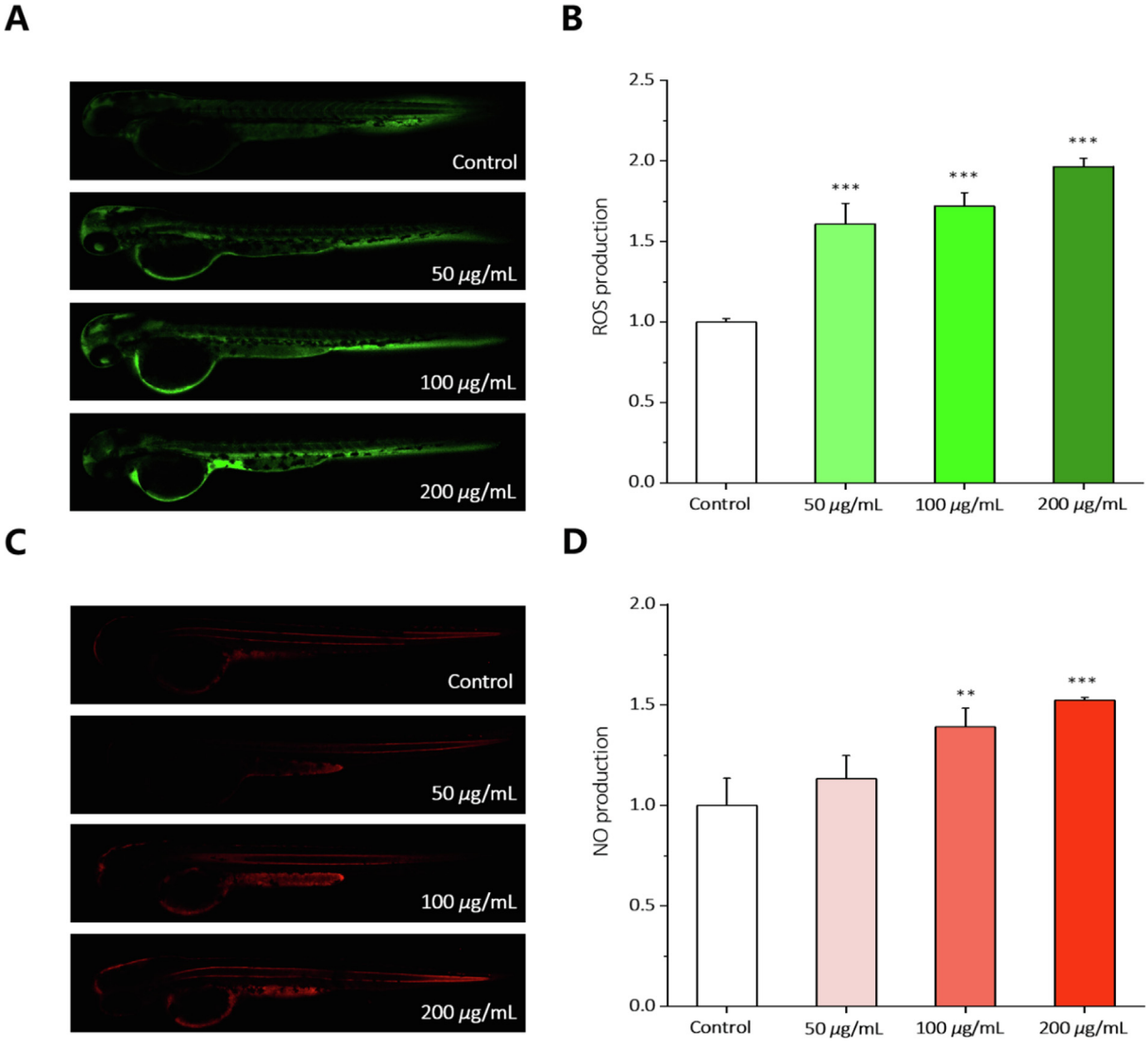

Fig. 8 Effects of PLP90-1B on ROS and NO production in zebrafish embryos. (A) The embryos were treated with PLP90-1B (50, 100, and 200 μg/mL) for 24 h and stained by DCFH-DA at 3 dpf. (B) Quantification of the relative fluorescence intensity of ROS. (C) The embryos were treated with PLP90-1B (50, 100, and 200 μg/mL) for 24 h and stained by DAF-FMDA at 3 dpf. (D) Quantification of the relative fluorescence intensity of NO. Each experiment was repeated three times and the results were expressed as mean ± SD. $^{**}P < 0.01$, $^{***}P < 0.001$ versus the control group.

concentration of PLP90-1B, the amount of ROS was 61 % (50 μg/mL), 72 % (100 μg/mL), and 97 % (200 μg/mL), which exceeded the control group (Fig. 8B), respectively. These results demonstrated that PLP90-1B could induce ROS release dose-dependently ($P < 0.001$). Simultaneously, PLP90-1B had the similar concentration-dependent effects on the NO release (Fig. 8D) *in vivo*. Higher dosages (100 and 200 μg/mL) of PLP90-1B caused remarkable increases of NO level ($P < 0.01$), which were 1.39 and 1.52 folds of the control group.

3.8. Structure-activity relationship analysis

The immunostimulation of polysaccharides on macrophages depends on the recognition of receptors. The foundation of recognition is dependent on the structural characteristics of polysaccharides including molecular weights, monosaccharide types, and glycosidic bond types (Yi et al., 2015). It has been found that arabinose has a positive effect on immunostimulation (Yi et al., 2018). Molecular weight affects the immunostimulatory activity and polysaccharides with molecular weight of 5–2400 kDa often have immunostimulatory effects (Zhang et al., 2016). The monosaccharide composition and molecular weight of PLP90-1B might contribute to the better immunoregulatory activity of PLP90-1B. Additionally, toll-like receptor 4 (TLR-4) has been shown to be an important polysaccharide receptor (Xu et al., 2020; Zhang et al., 2022a). Polysaccharides that activate TLR-4 mainly contain α-(1, 3), α-(1, 4), β-(1, 3), and β-(1, 4) glycosidic bonds (Camelini et al., 2005; Zhang et al., 2016). PLP90-1B contained α-(1, 4) glycosidic bonds, which might directly affect macrophages through TLR4 signal pathway to enhance immunomodulation, thus indirectly exerting anti-tumor effects.

4. Conclusions

In summary, a homogeneous polysaccharide (PLP90-1B) was successfully extracted and purified from *P. lactiflora*, which was a heteropolysaccharide and mainly consisted of arabinose and glucose. The main linkage patterns of PLP90-1B were proven to be → 5)-α-L-Ara*f*-(1→, →3,5)-α-L-Ara*f*-(1→, →2,3,5)-α-L-Ara*f*-(1→, and → 4)-α-D-Glc*p*-(1→, terminating with t-α-L-Ara*f*. The anti-tumor biological evaluation revealed that PLP90-1B displayed remarkable anti-tumor effects *in vivo* by suppressing proliferation and migration of tumor cells effectively in zebrafish xenografts. The subsequent anti-proliferation and immunomodulation experiments revealed the anti-tumor effects of PLP90-1B were closely related to immune regulation. PLP90-1B exhibited significant immune regulation *in vitro* and *in vivo*, which can enhance the phagocytosis of macrophages, promote the release of NO, TNF-α, IL-6 and IL-1β, and stimulate the release of ROS and NO in zebrafish. Taken together, this study provides experimental support for the polysaccharide fraction from *P. lactiflora* as an immunoregulation-based anti-tumor agent, which may be potential useful for cancer treatment.

5. Author agreement

Each author has completed the corresponding work, and there is no conflict of interest between the authors. The undersigned declare that this manuscript is original, has not been published before and is not currently being considered for publication elsewhere. We confirm that the manuscript has been read and approved by all named authors and that there are no other persons who satisfied the criteria for authorship but are not listed. We further confirm that the order of authors listed in the manuscript has been approved by all of us. We understand that the Corresponding Author is the sole contact for the Editorial process. He/she is responsible for communicating with the other authors about progress submissions of revisions and final approval of proofs.

CRediT authorship contribution statement

Xuelian Wang: . **Na Li:** . **Ying Li:** . **Yinan Zhao:** Writing – review & editing. **Liang Zhang:** Conceptualization, Funding acquisition, Project administration, Methodology, Supervision. **Yanjun Sun:** Writing – review & editing. **Yasushi Ohizumi:** Writing – review & editing. **Jing Xu:** Conceptualization, Funding acquisition, Project administration, Methodology, Supervision. **Yuanqiang Guo:** Conceptualization, Funding acquisition, Project administration, Methodology, Supervision.

Declaration of Competing Interest

The authors declare that they have no known competing financial interests or personal relationships that could have appeared to influence the work reported in this paper.

Acknowledgments

This research was supported financially by the National Natural Science Foundation of China (Nos. 22077067 and U1801288), and the Open Fund of State Key Laboratory of Tea Plant Biology and Utilization (SKLTOF20190114), Anhui Agricultural University.

Appendix A. Supplementary data

Supplementary data to this article can be found online at https://doi.org/10.1016/j.arabjc.2022.104132.

References

Bhardwaj, M., Mani, S., Malarvizhi, R., Sali, V.K., Vasanthi, H.R., 2021. Immunomodulatory activity of brown algae *Turbinaria ornata* derived sulfated polysaccharide on LPS induced systemic inflammation. Phytomedicine 89, 153615.

Camelini, C.M., Maraschin, M., Mendonca, M.M., Zucco, C., Ferreira, A.G., Tavares, L.A., 2005. Structural characterization of beta-glucans of *Agaricus brasiliensis* in different stages of fruiting body maturity and their use in nutraceutical products. Biotechnol. Lett. 27, 1295–1299.

Chen, Z., Zhao, Y., Zhang, M., Yang, X., Yue, P., Tang, D., Wei, X., 2019. Structural characterization and antioxidant activity of a new polysaccharide from *Bletilla striata* fibrous roots. Carbohydr. Polym. 227, 115362.

Cheng, X., Shi, S., Su, J., Xu, Y., Ordaz-Ortiz, J.J., Li, N., Wu, J., Wang, S., 2020. Structural characterization of a heteropolysaccharide from fruit of *Chaenomelese speciosa* sweet Nakai and its antitumor activity. Carbohydr. Polym. 236, 116065.

Ciucanu, I., Kerek, F., 1984. A simple and rapid method for the permethylation of carbohydrates. Carbohyd. Res. 131, 209–217.
Fan, Y., Xue, W., Schachner, M., Zhao, W., 2018. Honokiol eliminates glioma/glioblastoma stem cell-like cells via JAK-STAT3 signaling and inhibits tumor progression by targeting epidermal growth factor receptor. Cancers. 11, 22.
Han, X., Hu, S., Yang, Q., Sang, X., Tang, D., Cao, G., 2021. Paeoniflorin ameliorates airway inflammation and immune response in ovalbumin induced asthmatic mice: From oxidative stress to autophagy. Phytomedicine 30, 153835.
Hui, H., Gao, W., 2022. Physicochemical features and antioxidant activity of polysaccharides from Herba *Patriniae* by gradient ethanol precipitation. Arabian J. Chem. 15, 103770.
Ko, E.Y., Heo, S.J., Cho, S.H., Lee, W.W., Kim, S.Y., Yang, H.W., Ahn, G., Cha, S.H., Kwon, S.H., Jenog, M.S., Lee, K.P., Jeon, Y. J., Kim, K.N., 2019. 3-Bromo-5-ethoxymethyl-1,2-benzenediol inhibits LPS-induced pro-inflammatory responses by preventing ROS production and downregulating NF-κB *in vitro* and in a zebrafish model. Int. Immunopharmacol. 67, 98–105.
Li, Z., An, L., Zhang, S., Shi, Z., Bao, J., Tuerhong, M., Abudukeremu, M., Xu, J., Guo, Y., 2021. Structural elucidation and immunomodulatory evaluation of a polysaccharide from *Stevia rebaudiana* leaves. Food Chem. 364, 130310.
Li, C., Dong, Z., Zhang, B., Huang, Q., Liu, G., Fu, X., 2020. Structural characterization and immune enhancement activity of a novel polysaccharide from *Moringa oleifera* leaves. Carbohydr. Polym. 234, 115897.
Liu, H.M., Liu, X.Y., Yan, Y.Y., Gao, J.H., Qin, Z., Wang, X.D., 2021. Structural properties and antioxidant activities of polysaccharides isolated from sunflower meal after oil extraction. Arabian J. Chem. 14, 103420.
Ma, J.S., Liu, H., Han, C.R., Zeng, S.J., Xu, X.J., Lu, D.J., He, H.J., 2019. Extraction, characterization and antioxidant activity of polysaccharide from *Pouteria campechiana* seed. Carbohydr. Polym. 229, 115409.
Mandal, E.K., Mandal, S., Maity, S., Behera, B., Maiti, T.K., Islam, S. S., 2013. Structural studies of an immunostimulating gluco-arabinan from seeds of *Caesalpinia bonduc*. Carbohydr. Polym. 92, 704–711.
Meng, Q., Meng, W., Bian, H., Zheng, F., Gu, H., Zuo, R., Miao, X., Zhou, Z., Wang, L.i., Wen, Z., Ma, J., Su, X., 2021. Total glucosides of paeony protects THP-1 macrophages against monosodium urate-induced inflammation via MALAT1/miR-876-5p/NLRP3 signaling cascade in gouty arthritis. Biomed. Pharmacother. 138, 111413.
Mohsenzadeh, M.S., MarjanRazavi, B., Imenshahidi, M., Yazdi, S.A. T., Mohajeri, S.A., Hosseinzadeh, H., 2021. Potential role of green tea extract and epigallocatechin gallate in preventing bisphenol A-induced metabolic disorders in rats: Biochemical and molecular evidence. Phytomedicine 92, 153754.
Molaei, H., Jahanbin, K., 2018. Structural features of a new water-soluble polysaccharide from the gum exudates of *Amygdalus scoparia* Spach Zedo gum. Carbohydr. Polym. 182, 98–105.
Patra, S., Maity, P., Chakraborty, I., Sen, I.K., Bhanja, S.K., 2021. Structural studies of immunomodulatory 1→3-, 1→4-α glucan from an edible mushroom *Polyporus grammocephalus*. Int. J. Biol. Macromol. 168, 649–655.
Shakhmatov, E.G., Toukach, P.V., Michailowa, E.A., Makarova, E. N., 2014. Structural studies of arabinan-rich pectic polysaccharides from *Abies sibirica* L. Biological activity of pectins of *A. sibirica*. Carbohydr. Polym. 113, 515–524.
Sheng, Z., Wen, L., Yang, B., 2022. Structure identification of a polysaccharide in *mushroom Lingzhi* spore and its immunomodulatory activity. Carbohydr. Polym. 15, 118939.
Shi, Z., An, L., Zhang, S., Li, Z., Li, Y., Cui, J., Zhang, J., Jin, D.Q., Tuerhong, M., Abudukeremu, M., Xu, J., Guo, Y., 2020. A heteropolysaccharide purified from leaves of *Ilex latifolia* displaying immunomodulatory activity *in vitro* and *in vivo*. Carbohydr. Polym. 245, 116469.
Song, J., Wu, Y., Ma, X., Feng, L., Wang, Z., Jiang, G., Tong, H., 2020. Structural characterization and α-glycosidase inhibitory activity of a novel polysaccharide fraction from *Aconitum coreanum*. Carbohydr. Polym. 230, 115586.
Tabarsa, M., You, S.G., Yelithao, K., Palanisamy, S., Prabhu, N.M., Nan, M., 2020. Isolation, structural elucidation and immunostimulatory properties of polysaccharides from *Cuminum cyminum*. Carbohydr. Polym. 230, 115636.
Tang, X., Huang, J., Xiong, H., Zhang, K., Chen, C., Wei, X., Xu, X., Xie, Q., Huang, R., 2016. Anti-tumor effects of the polysaccharide isolated from *Tarphochlamys Affinis* in H22 tumor-bearing mice. Cell Physiol. Biochem. 39, 1040–1050.
Wang, N., Jia, G., Wang, X., Liu, Y., Li, Z., Bao, H., Guo, Q., Wang, C., Xiao, D., 2020. Fractionation, structural characteristics and immunomodulatory activity of polysaccharide fractions from asparagus *Asparagus officinalis* L. skin. Carbohydr. Polym. 256, 117514.
Wang, H., Wang, X., Li, Y., Zhang, S., Li, Z., Li, Y., Cui, J., Lan, X., Zhang, E., Yuan, L., Jin, D.Q., Tuerhong, M., Abudukeremu, M., Xu, J., Guo, Y., 2021a. Structural properties and *in vitro* and *in vivo* immunomodulatory activity of an arabinofuranan from the fruits of *Akebia quinata*. Carbohydr. Polym. 256, 117521.
Wang, H., Wang, X., Zhou, L., Zhang, S., An, L., Bao, J., Li, Z., Sun, Y., Li, Y., Cui, J., Jin, D.Q., Zhang, J., Xu, J., Guo, Y., 2021b. Structural characteristics and *in vitro* and *in vivo* immunoregulatory properties of a gluco-arabinan from *Angelica dahurica*. Int. J. Biol. Macromol. 183, 90–100.
Wang, H., Li, Y., Wang, X., Li, Y., Cui, J., Jin, D.Q., Tuerhong, M., Abudukeremu, M., Xu, J., Guo, Y., 2022. Preparation and structural properties of selenium modified heteropolysaccharide from the fruits of Akebia quinata and in vitro and in vivo antitumor activity. Carbohydr. Polym. 278, 118950.
Wang, M., Zhao, S., Zhu, P., Nie, C., Ma, S., Wang, N., Du, X., Zhou, Y., 2018. Purification, characterization and immunomodulatory activity of water extractable polysaccharides from the swollen culms of *Zizania latifolia*. Int. J. Biol. Macromol. 107, 882–890.
Xie, X., Zhou, Y., Wang, X., Guo, J., Li, J., Fan, H., Dou, J., Shen, B., Zhou, C., 2017. Enhanced antitumor activity of gemcitabine by polysaccharide-induced NK cell activation and immune cytotoxicity reduction *in vitro*/*vivo*. Carbohydr. Polym. 173, 360–371.
Xu, Z., Lin, R., Hou, X., Wu, J., Zhao, W., Ma, H., Fan, Z., Li, S., Zhu, Y., Zhang, D., 2020. Immunomodulatory mechanism of a purified polysaccharide isolated from *Isaria cicadae* Miquel on RAW264.7 cells via activating TLR4-MAPK-NF-κB signaling pathway. Int. J. Biol. Macromol. 164, 4329–4338.
Yi, Y., Wang, H., Zhang, R., Min, T., Huang, F., Liu, L., Zhang, M., 2015. Characterization of polysaccharide from longan pulp as the macrophage stimulator. RSC Adv. 5, 97163–97170.
Yi, Y., Lamikanra, O., Sun, J., Wang, L.M., Min, T., Wang, H.X., 2018. Activity diversity structure-activity relationship of polysaccharides from lotus root varieties. Carbohydr. Polym. 190, 67–76.
Yu, W., Zeng, M., Xu, P., Liu, J., Wang, H., 2021. Effect of paeoniflorin on acute lung injury induced by influenza A virus in mice. Evidences of its mechanism of action. Phytomedicine 92, 153724.
Zeinali, M., Rezaee, S.A., Hosseinzadeh, H., 2017. An overview on immunoregulatory and anti-inflammatory properties of chrysin and flavonoids substances. Biomed. Pharmacother. 92, 998–1009.
Zhang, B., Lu, C., Xu, Z., Guo, H., Zhang, G., Hao, Y., 2022a. The effect of *Moringa oleifera* polysaccharides on the regulation of glucocorticoid-induced femoral head necrosis: In vitro and in vivo. Arabian J. Chem. 15, 103410.
Zhang, J., Song, Z., Li, Y., Zhang, S., Bao, J., Wang, H., Dong, C., Ohizumi, Y., Xu, J., Guo, Y., 2021a. Structural analysis and

biological effects of a neutral polysaccharide from the fruits of *Rosa laevigata*. Carbohydr. Polym. 265, 118080.

Zhang, M., Yan, M., Yang, J., Li, F., Wang, Y., Feng, K., Wang, S., Lin, N., Wang, Y., Yang, B., 2022b. Structural characterization of a polysaccharide from *Trametes sanguinea* Lloyd with immune-enhancing activity via activation of TLR4. Int. J. Biol. Macromol. 206, 1026–1038.

Zhang, S., Zhang, Q., An, L., Zhang, J., Li, Z., Zhang, J., Li, Y., Tuerhong, M., Ohizumi, Y., Jin, J., Xu, J., Guo, Y., 2020a. A fructan from *Anemarrhena asphodeloides* bunge showing neuro-protective and immunoregulatory effects. Carbohydr. Polym. 229, 115477.

Zhang, S., An, L., Li, Z., Wang, X., Wang, H., Shi, L., Bao, J., Lan, X., Zhang, E., Lall, N., Reid, A., Li, Y., Jin, D.Q., Xu, J., Guo, Y., 2021b. Structural elucidation of an immunological arabinan from the rhizomes of *Ligusticum chuanxiong*, a traditional Chinese medicine. Int. J. Biol. Macromol. 170, 42–52.

Zhang, W., Hu, Y., Zhao, J., Zhang, Y., Guo, D., Gao, C., Duan, J., Li, P., 2020b. Immunoregulation and antioxidant activities of a novel acidic polysaccharide from *Radix Paeoniae* Alba. Glycoconjugate J. 37, 361–371.

Zhang, X., Qi, C., Guo, Y., Zhou, W., Zhang, Y., 2016. Toll-like receptor 4-related immunostimulatory polysaccharides: Primary structure, activity relationships, and possible interaction models. Carbohydr. Polym. 149, 186–206.

Zhu, Y., Cai, Y., Cao, X., Li, P., Liu, D., Ye, S., Xu, Z., Shen, B., Liao, Q., Li, H., Xie, Z., 2022. Structural analysis and immunomodulatory activity of a homopolysaccharide isolated from *Parabacteroides distasonis*. Arabian J. Chem. 15, 103755.